# Supporting Information

# $CeO_2$-regulated NiCoOOH formed via electrocatalytic self-reconstruction of NiCoCe-MOFs for efficient electro-oxidation of 5-hydroxymethylfurfural

Hao Pan,[a] Gongchi Zhao,[a] Guangtong Hai,[b*] Baoxiang Peng,[c] Fengyu Gao,[d] Cheng Zhang,[e] Yan Wang,[e] Xiubing Huang*[a]

[a] Beijing Advanced Innovation Center for Materials Genome Engineering, Beijing Key Laboratory of Function Materials for Molecule & Structure Construction, School of Materials Science and Engineering, University of Science and Technology Beijing, Beijing 100083, P. R. China

[b] Institute of Zhejiang University-Quzhou, Zhejiang University, 99 Zheda Road, Quzhou, Zhejiang Province 324000, P. R. China

[c] Laboratory of Industrial Chemistry, Ruhr University Bochum, 44780 Bochum, Germany

[d] School of Energy and Environmental Engineering, University of Science and Technology Beijing, Beijing 100083, P. R. China

[e] Baotou Research Institute of Rare Earths, Baotou 014030, P. R. China

* Corresponding authors: haigt@zju.edu.cn (G. Hai), xiubinghuang@ustb.edu.cn (X. Huang)

**Chemicals and Materials**

All chemicals and materials were utilized exactly as received, with no further purification. Nickel nitrate hexahydrate [$Ni(NO_3)_2 \cdot 6H_2O$, AR] and acetone [$C_3H_6O$, AR] were purchased from Sinopharm Chemical Reagent Co., Ltd. Cobaltous nitrate hexahydrate [$Co(NO_3)_2 \cdot 6H_2O$, 99.99%] was purchased from AI LAN (Shanghai) Chemical Technology Co., Ltd. Terephthalic acid [$C_8H_6O_4$, 99%] was purchased from Beijing InnoChem Science & Technology Co., Ltd. N,N-Dimethylmethanamide [DMF, AR] and hydrochloric acid [HCl, GR] was purchased from Beijing Tongguang Fine Chemical Co., Ltd. Cerium(III) nitrate hexahydrate [$Ce(NO_3)_3 \cdot 6H_2O$, 99.5%] was purchased from Thermo Fisher Scientific (China) Co., Ltd. 5-Hydroxymethylfurfural [HMF, 99.54%], furan-2,5-dicarbaldehyde [DFF, 98%] were purchased from Ark Pharma Scientific Co., Ltd. Potassium hydroxide [KOH, 95%], 5-hydroxymethyl-2-furancarboxylic acid [HMFCA, 98%], 5-formyl-2-furancarboxylic acid [FFCA, >98%], 2,5-furandicarboxylic acid [FDCA, 98%] were purchased from Shanghai Aladdin Bio-Chem Technology Co., Ltd. Nickel foam [NF, 350 ± 25 g/m$^2$] was purchased from Beijing Tianmei Hechuang Technology Co., Ltd.

**Synthesis**

NiCoCe-MOF was synthesized by improving the reported method of MOF synthesis. First, a clean piece of nickel foam (NF) (2 × 4 cm$^2$) was treated with 1 M HCl, acetone, and deionized water in an ultrasonic bath for 15 min each, and then transferred to a vacuum drying oven to dry overnight to obtain pretreated NF. Then 2.667 mmol (0.776 g) $Ni(NO_3)_2 \cdot 6H_2O$, 1.333 mmol (0.383 g) $Co(NO_3)_2 \cdot 6H_2O$ and 0.3 mmol (0.130 g) $Ce(NO_3)_3 \cdot 6H_2O$ were dissolved in 20 mL DMF and kept stirring until the solution was transparent, which was named A solution. Dissolve 4.3 mmol (0.714 g) $H_2BDC$ in 20 mL DMF, slowly add 4 mL of 0.4 M NaOH solution dropwise during stirring, and name it B solution. After solution B was stirred to milky white, quickly pour solution B into solution A and stir for 5 min. The stirred solution, together with the pre-treated NF, was then transferred to a 50 mL polyfluoroethylene (PTFE) reactor and heated at 100 °C for 15 hours. After the reaction was completed and the reactor was cooled to room temperature, the samples were washed several times with DMF and dried overnight in a vacuum drying oven. The obtained sample was named NiCoCe-MOF. In the hydrothermal process, except that $Ce(NO_3)_3 \cdot 6H_2O$ was not added and the molar amount of $H_2BDC$ was adjusted to 4 mmol, other synthesis steps were consistent with those of NiCoCe-MOF, and the obtained sample was named NiCo-MOF. In 1.0 M KOH electrolyte, NiCoCe-MOF and NiCoCe-MOF were treated by cyclic voltammetry for 80 cycles in the potential range of 0.925 - 1.725 $V_{RHE}$, and the samples obtained by vacuum drying overnight were named NiCoOOH and $CeO_2$/NiCoOOH, respectively.

**Characterizaiton**

The morphology and microstructure were obtained by field emission scanning electron microscopy (FE-SEM, Hitachi SU8010, Japan) and transmission electron microscopy (TEM, JEM-2200FS, Japan). The X-ray diffraction (XRD) patterns were acquired through a Bruker D8 ADVANCE with Cu Kα radiation (λ = 1.5406 Å) at 40 kV and 40 mA. X-ray photoelectron spectroscopy (XPS, Thermo Scientific ESCALAB 250Xi, USA) was used to collect information on elements in composite materials. Fourier infrared spectroscopy (FTIR, Nicolet 6700) was used to collect functional group information in composite materials. High-resolution Raman spectrometer (LabRAM HR Evolution) (325 nm) was used to study the structural evolution during electrochemical processes. Synchronous thermal analyzer (TG-DSC, Netzsch STA449F3) was used to characterize the thermal decomposition behavior of the sample. Elemental contents were measured by inductively coupled plasma optical emission spectroscopy (ICP-OES, Agilent 5110 ICP-OES). The XAFS spectra were measured at room temperature on the BL14W1 baseline in the Shanghai Synchrotron Radiation Facility (SSRF)

**Electrochemical measurements**

Utilizing a CHI-660D electrochemical workstation (CHI Instrument, Shanghai, China) in a typical three-electrode cell configuration, all electrochemical experiments were carried out at room temperature. A piece of the prepared self-supported catalyst, graphite rod, and Hg/HgO were applied as working electrode, counter electrode, and reference electrode, respectively. The working electrolytes for OER process and HMFOR process were 1 M KOH (pH = 14) and 1.0 M KOH + 50 mM HMF (pH = 14), respectively. According to the Nernst equation, the measured potentials (vs. Hg/HgO) were stated concerning the reversible hydrogen electrode (RHE) scale: $E\ (_{vs.\ RHE}) = E\ (_{vs.\ Hg/HgO}) + 0.098 + 0.0591 \times pH$. Linear sweep voltammetry (LSV) curves with 90-iR compensation were collected at a scan rate of 5 mV $s^{-1}$. Electrochemical surface area (ECSA) is computed using the following formula: ECSA = Cdl/Cs. Here, Cdl indicates the double-layer capacitance acquired from CV cycles, whereas Cs is commonly used for Co-based catalysts as 0.04 mF $cm^{-2}$. The in situ electrochemical impedance spectroscopy (EIS) measurements were carried out in the frequency range of $10^5$ to $10^{-2}$ Hz with an AC amplitude of 5 mV. All electrochemical experiments in this experiment were carried out in a single-chambered immobile cell. The electrolysis of HMF was stirred using magnets, except for the other test experiments (LSV, Cdl, EIS, etc.) which were not stirred.

**HPLC analysis**

High-performance liquid chromatography (HPLC, Agilent 1260 Infinity Series, USA) with an ultraviolet-visible (UV-Vis) detector and an Agilent Zorbax SB-C18 (150 mm × 4.6 mm, 5 μm) column was used to identify and quantify the substrate (HMF), intermediates (HMFCA, FFCA and DFF), and final oxidation product (FDCA). In a typical experiment, 50 uL of electrolyte was collected

during potentiostatic electrolysis, diluted to 5 mL with deionized water, and analyzed using HPLC. In terms of analysis conditions, the UV-Vis detector had a wavelength of 265 nm. The mobile phases A and B were made up of chromatographic grade methanol and an aqueous solution of 5 mM ammonium formate, in a volume ratio of 3:7. The rate of flow was fixed at 0.6 mL $min^{-1}$. The column temperature was kept constant at 30 °C, and each separation lasted 10 minutes. To identify and quantify products, the external standard approach was utilized. This involved applying standard solutions with known concentrations of commercially available pure reactants, intermediates, and final products to obtain calibration curves.

The theoretical charge of the electrochemical oxidation reaction was calculated as follows:

$6 \times 10$ mM $\times$ 8 mL $\times$ 96485 C $mol^{-1}$ = 46.3 C

Equations (1), (2), and (3) are used to calculate HMF conversion, FDCA selectivity, and Faradaic efficiency, respectively.

$$\text{HMF conversion (\%)} = [n(\text{HMF consumed}) / n(\text{HMF initial})] \times 100 \quad (1)$$

$$\text{Product Yield (\%)} = [n(\text{certain product formed}) / n(\text{HMF initial})] \times 100 \quad (2)$$

$$\text{Faradaic efficiency (\%)} = [n(\text{FDCA formed}) / (\text{Charge} / (6 \times F))] \times 100 \quad (3)$$

where F denotes the Faraday constant (96485 C $mol^{-1}$) and n denotes the identified product's molar weight.

**Density functional theory calculations**

The Vienna ab initio simulation program (VASP) was used to compute spin-polarized density-functional theory (DFT) using the projector augmented wave (PAW) approach. The electron-ion interactions were characterized using typical PAW potentials. The smooth component of the wave functions with a cutoff kinetic energy of 450 eV was expanded using a plane-wave basis set. The Perdew-Burke-Ernzerhof (PBE) functional, a form of the General Gradient Approximation (GGA), has been used throughout the electron-electron exchange and correlation interactions. For the study of the mechanistic chemistry of surface reactions, the surface has been modelled with a slab model. The vacuum region of 15 Å was large enough to have a good separation of the periodic images. When calculating the surface properties during the geometry optimization, the bottom atoms were fixed in the bulk position. In this work, Monkhorst-Pack (MP) grids of special points with a separation of 0.04 $Å^{-1}$ were used for the Brillouin zone integrations. The convergence criterion for the electronic self-consistent loop was set to $10^{-5}$ eV. The atomic structures have been optimized until the residual forces are less than 0.03 eV $Å^{-1}$.

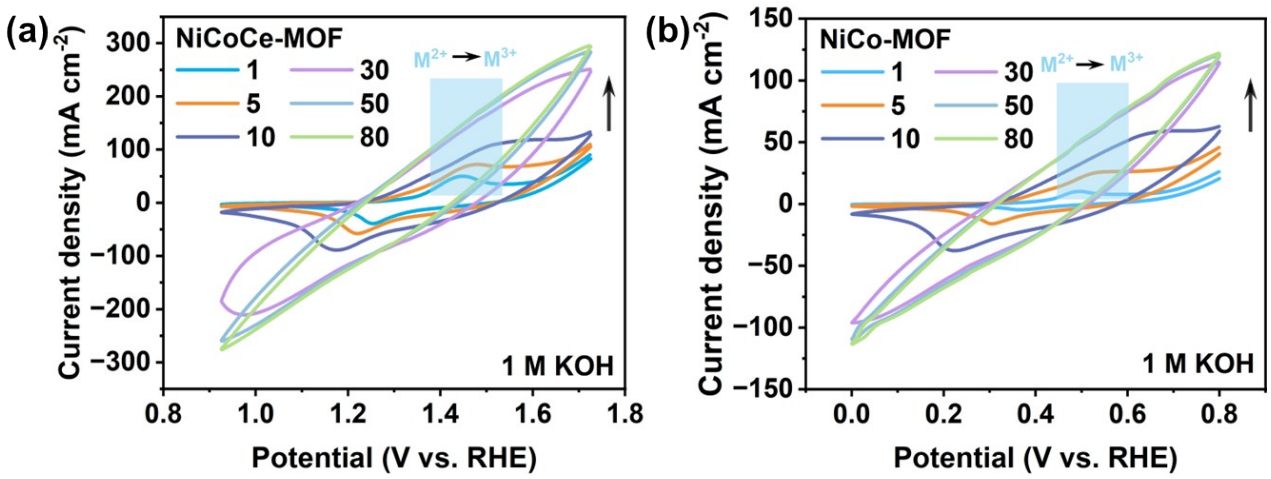


**Figure S1.** Detailed CV curves of (a) NiCo-MOF and (b) NiCoCe-MOF in 1 M KOH.

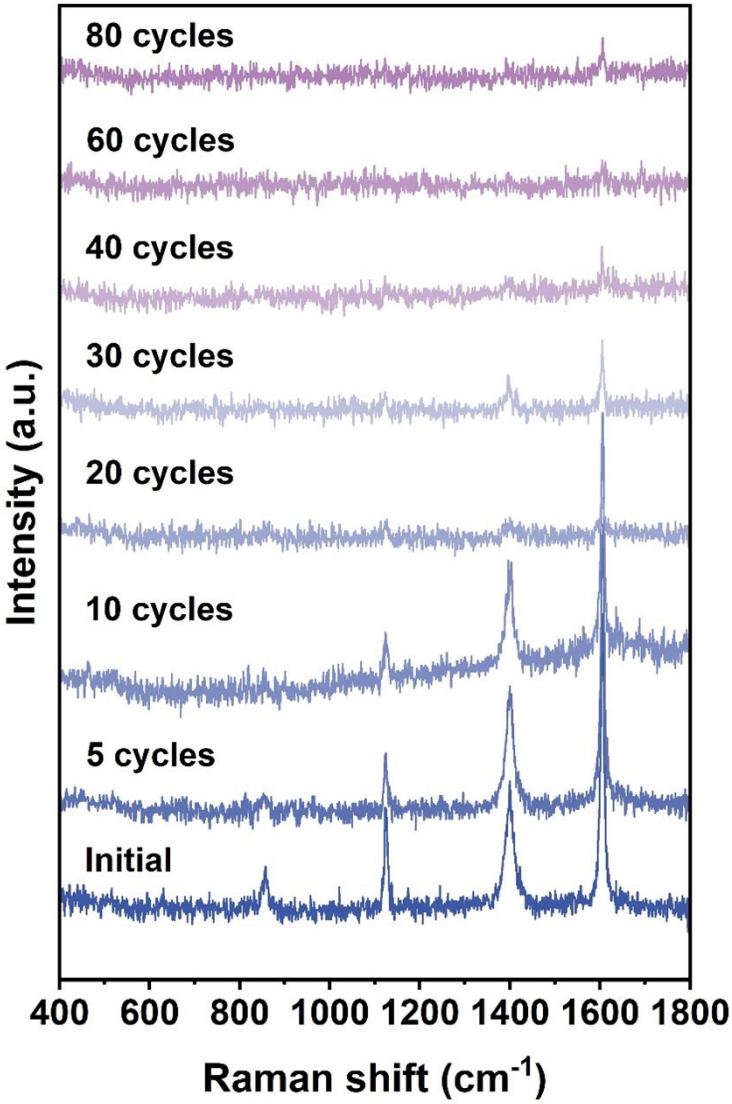


**Figure S2.** Raman mapping of NiCoCe-MOF during the CV process.

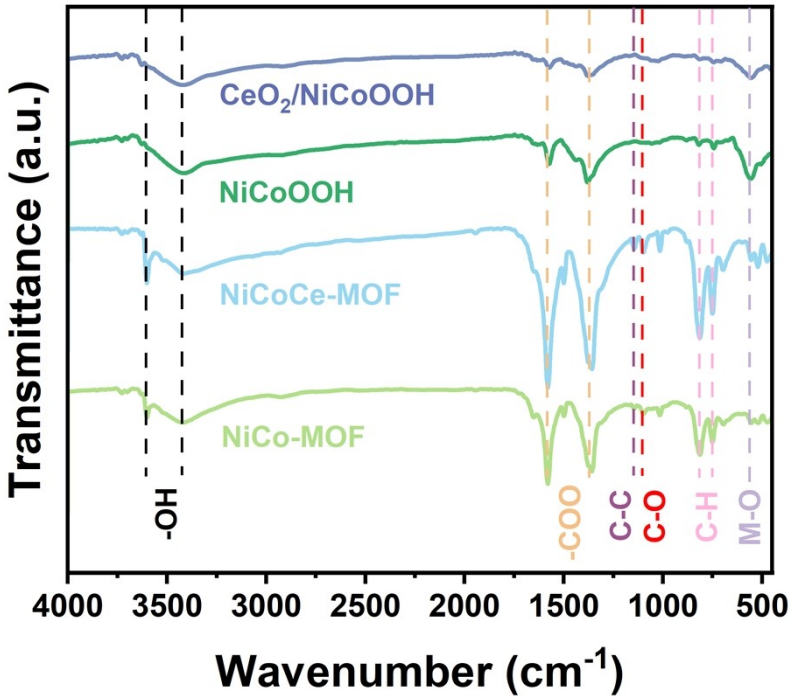


**Figure S3.** FT-IR spectra of NiCo-MOF, NiCoCe-MOF, NiCoOOH and $CeO_2$/NiCoOOH samples collected by sonication.

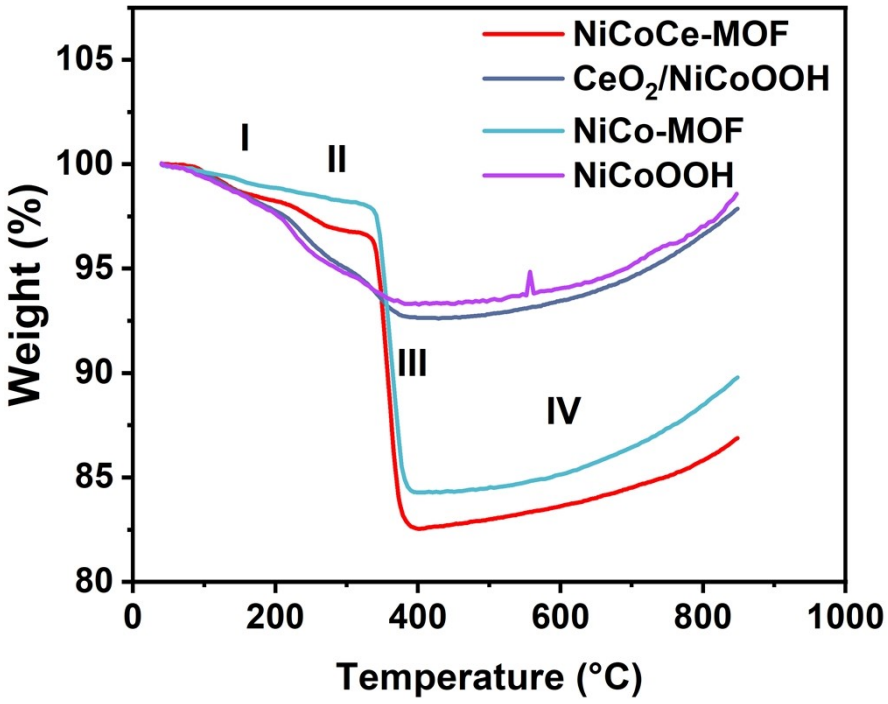


**Figure S4.** TG curves of NiCoCe-MOF and $CeO_2$/NiCoOOH samples collected by sonication.

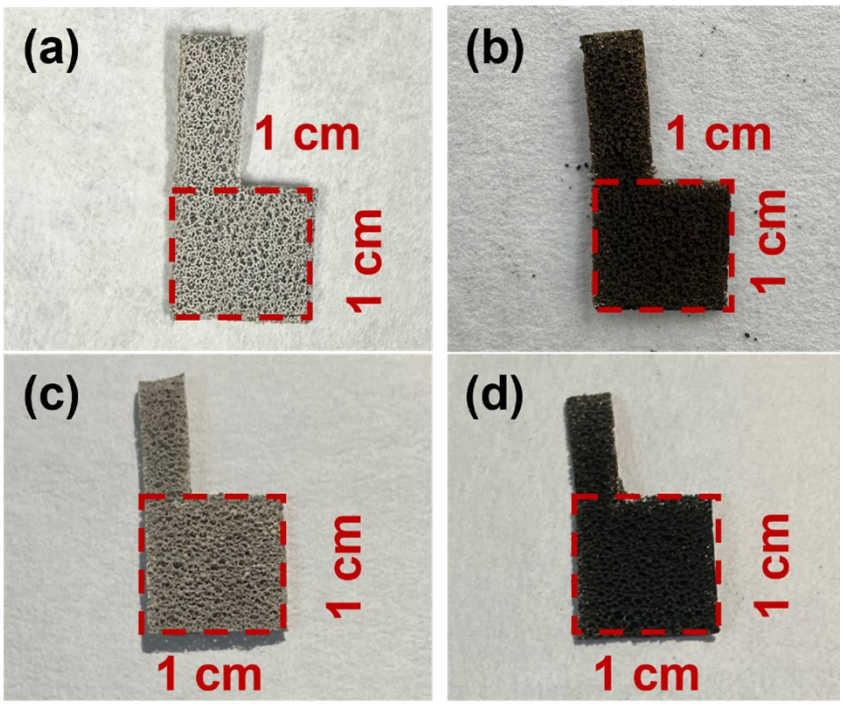


**Figure S5.** Optical photos of (a) NiCo-MOF, (b) NiCoOOH, (c) NiCoCe-MOF and (d) $CeO_2$/NiCoOOH.

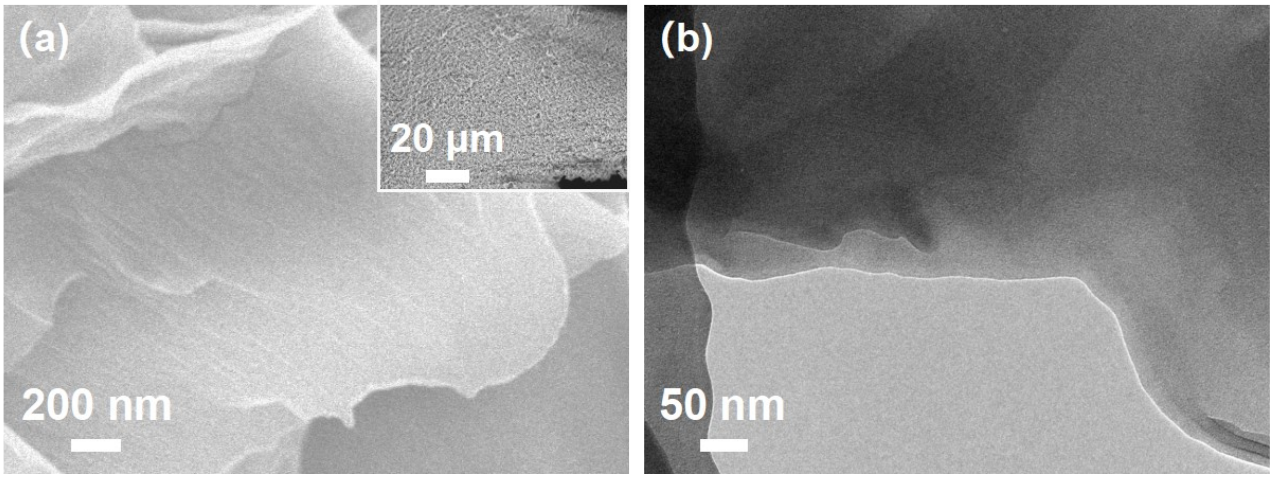


**Figure S6.** (a) SEM and (b) TEM images of NiCo-MOF.

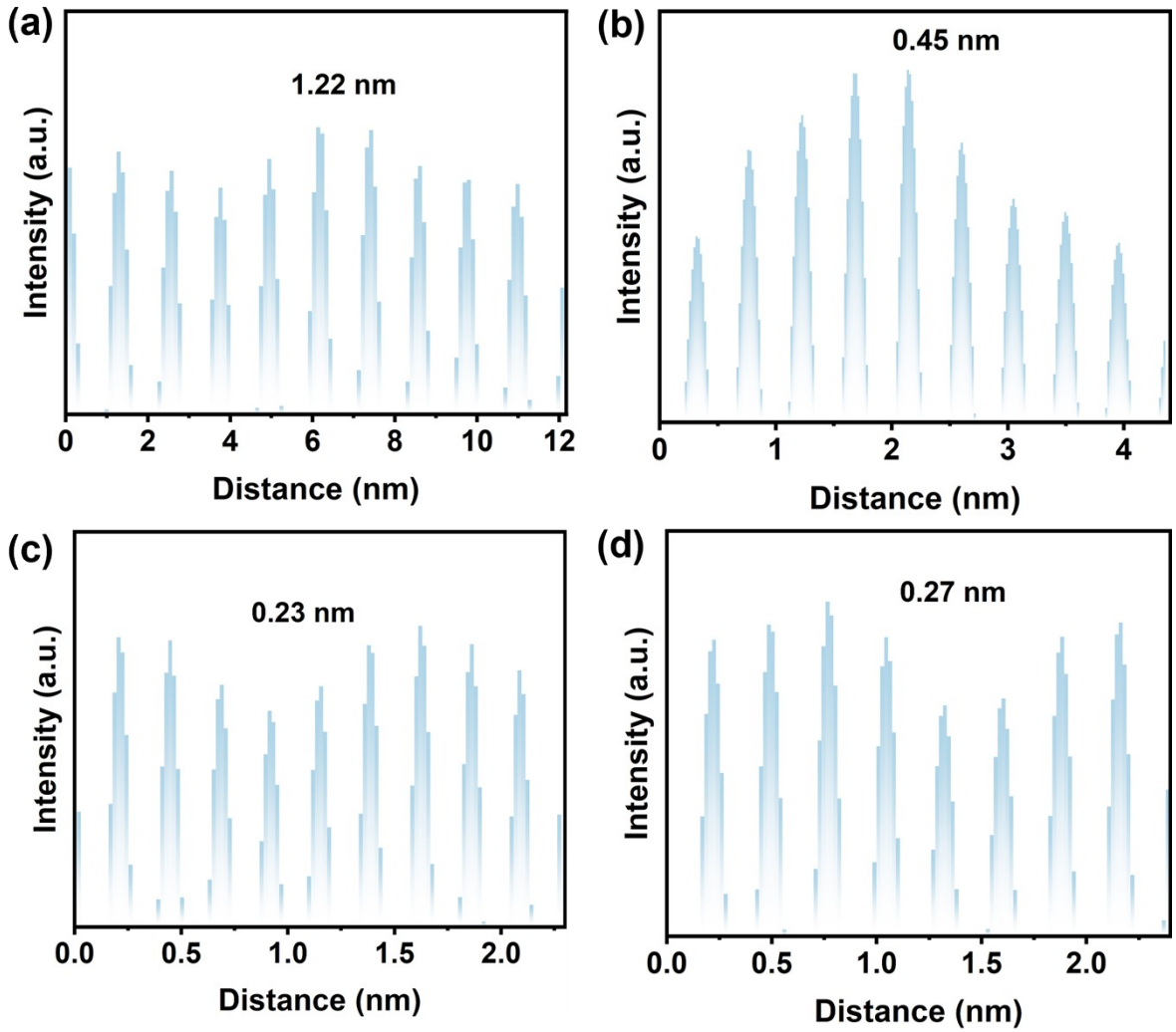


**Figure S7.** The corresponding interplanar spacing of (a) NiCoCe-MOF, (b) NiCoOOH (200) crystal plane, (c) NiCoOOH (020) crystal plane and (d) $CeO_2$ (200) crystal plane interplanar spacing of $CeO_2$/NiCoOOH.

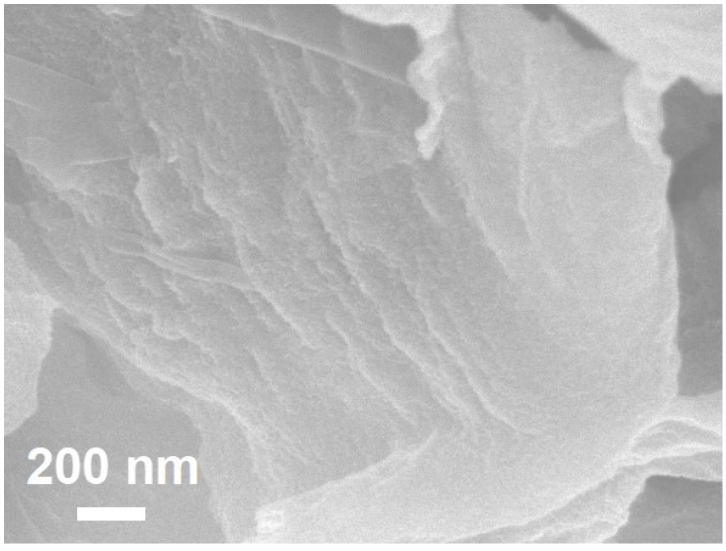


**Figure S8.** SEM image of NiCoOOH

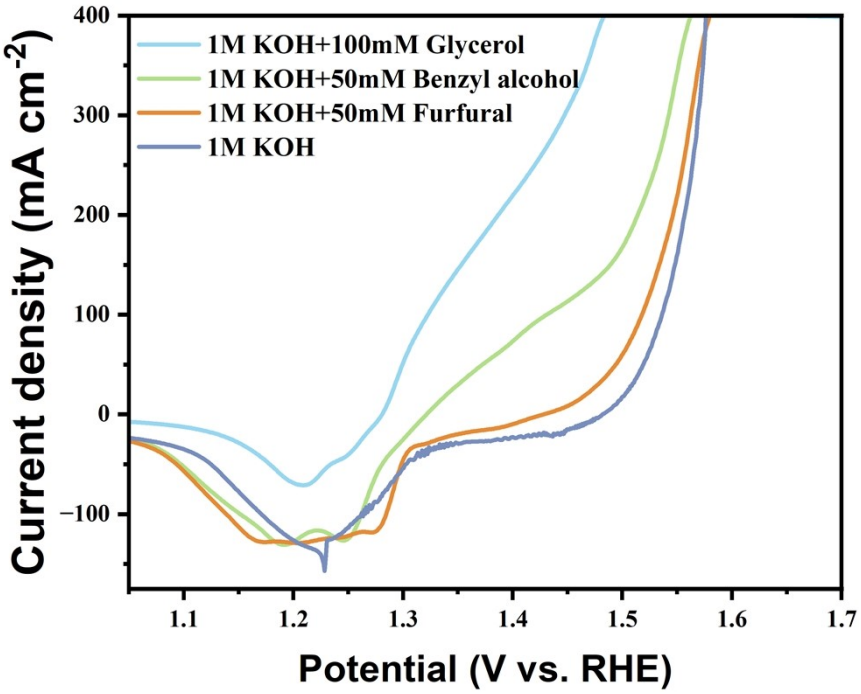


**Figure S9.** Electrooxidation activity of $CeO_2$/NiCoOOH LSV curves of the oxidation of glycerol, benzyl alcohol, furfuryl, and KOH.

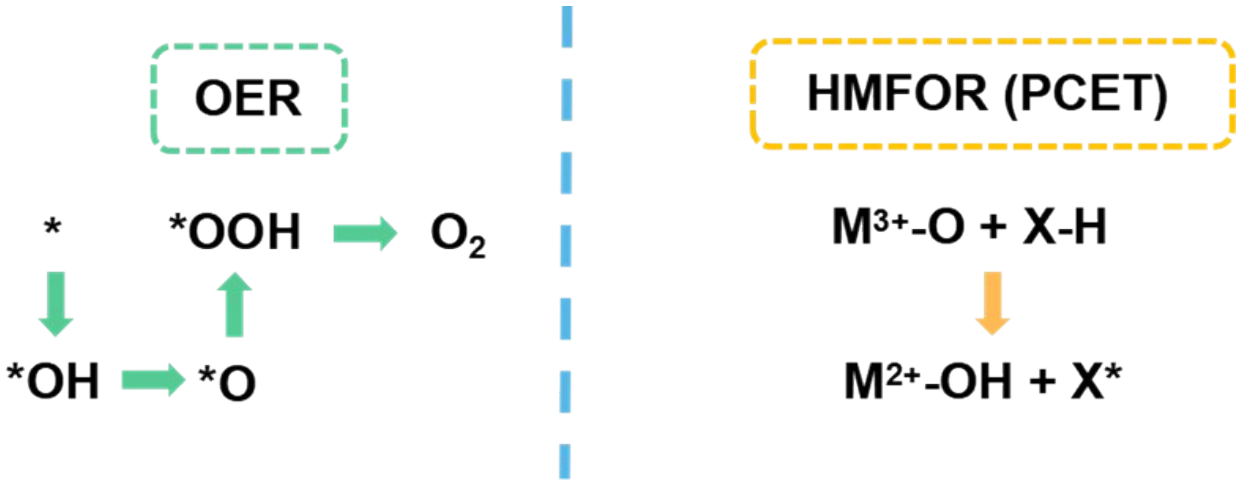


**Figure S10.** Schematic diagram of OER and HMFOR reactions.

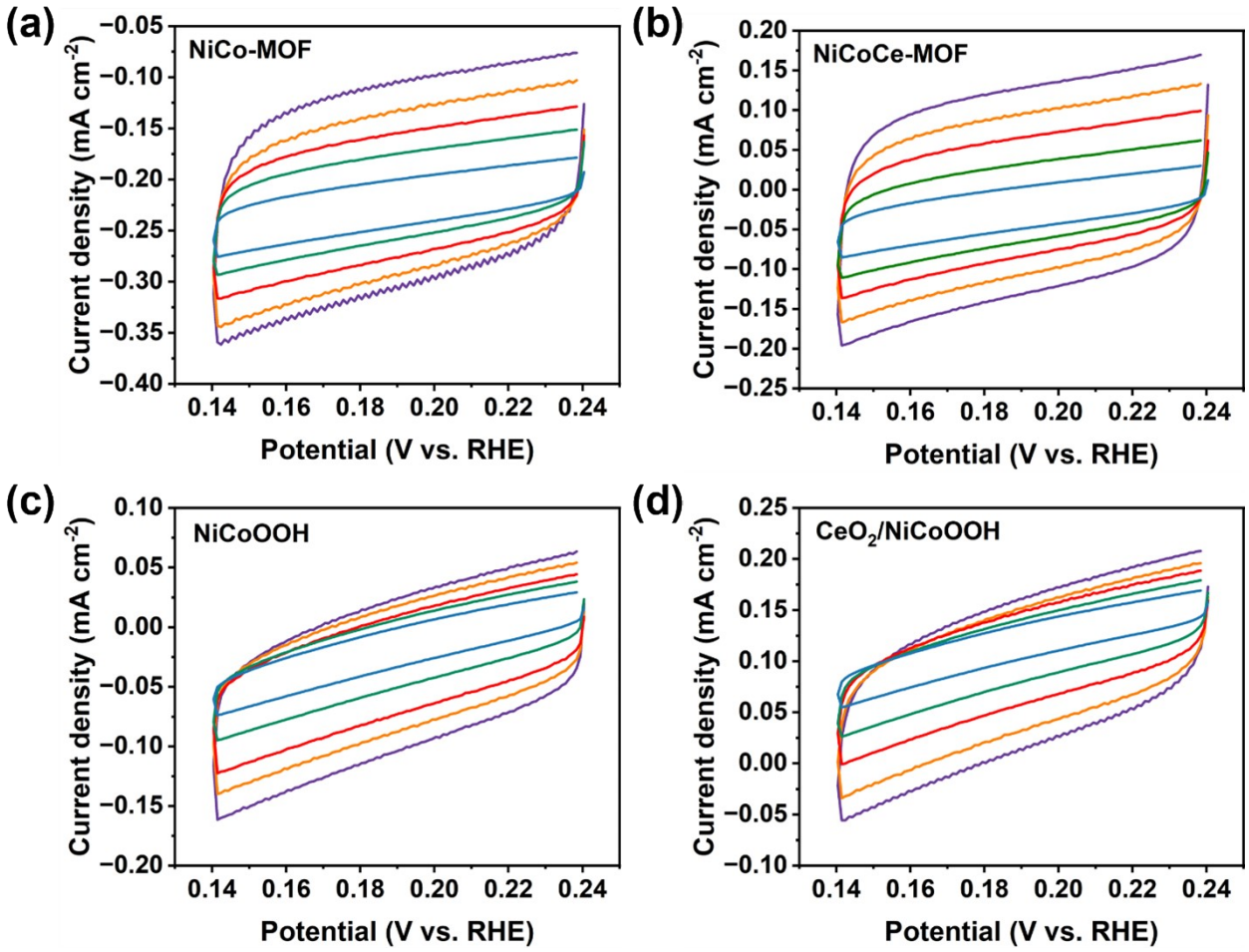


**Figure S11.** (a) NiCo-MOF ; (b) NiCoCe-MOF; (c) NiCoOOH and (d) $CeO_2$/NiCoOOH in CV cycles at different scanning rates.

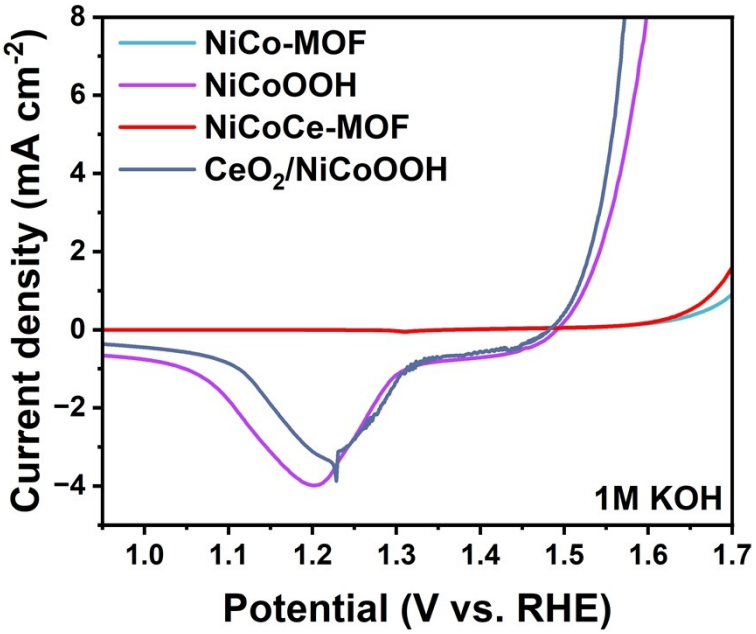


**Figure S12.** ECSA normalized LSV curves of NiCoOOH and $CeO_2$/NiCoOOH

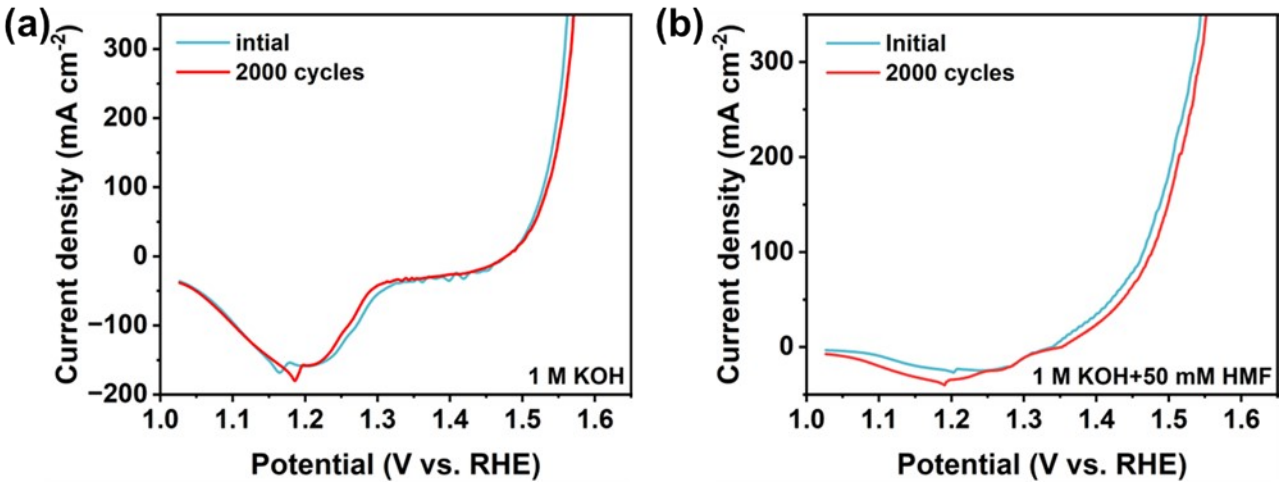


**Figure S13.** OER and HMFOR performance curves of $CeO_2$/NiCoOOH after 2000 cycles.

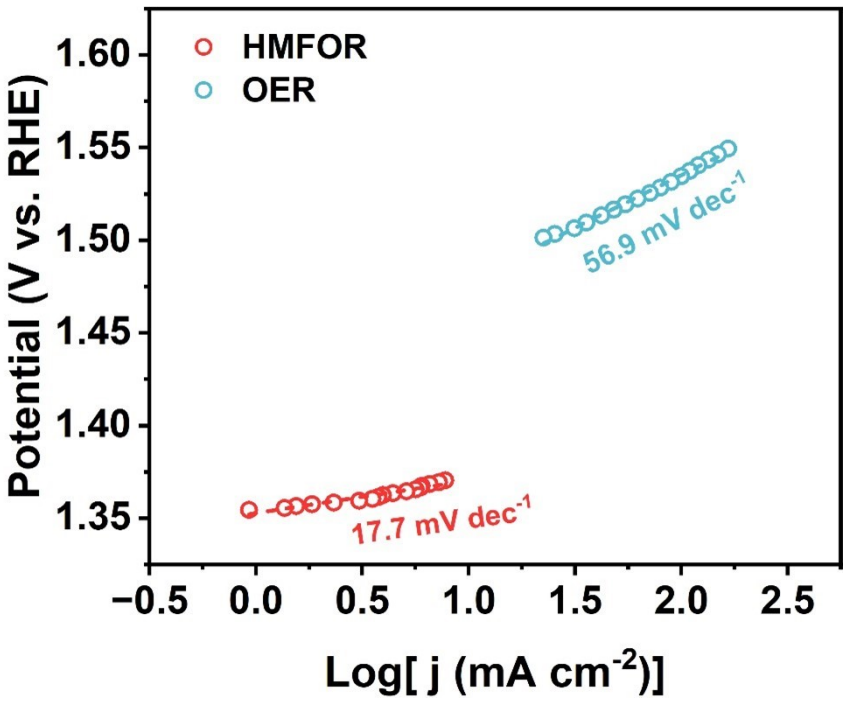


**Figure S14.** Tafel slope after 2000 cycles of $CeO_2$/NiCoOOH.

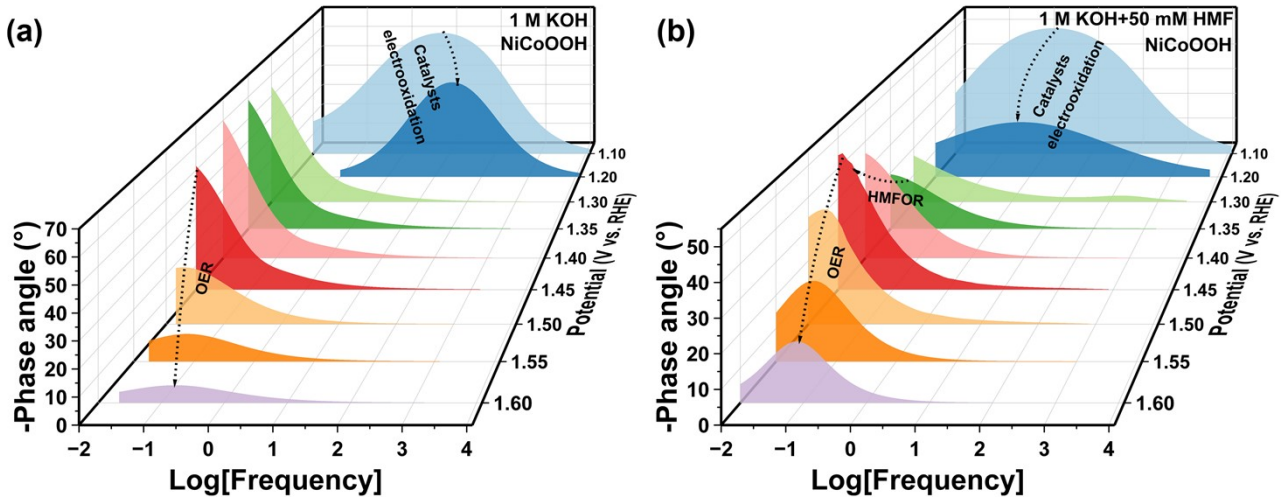


**Figure S15.** Bode plots of NiCoOOH at various potentials in (a) 1 M KOH and (b) 1 M KOH + 50 mM HMF.

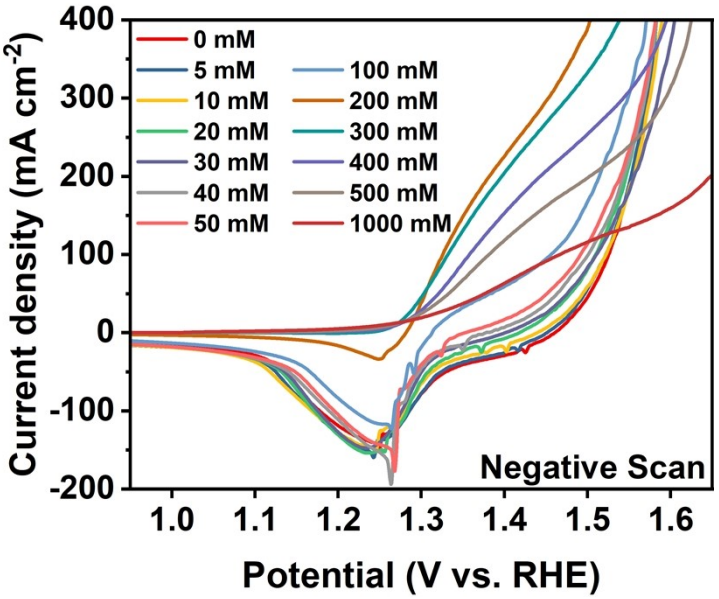


**Figure S16.** LSV curves of $CeO_2$/NiCoOOH in 1 M KOH electrolyte with varied concentrations of HMF (0-1000 mM).

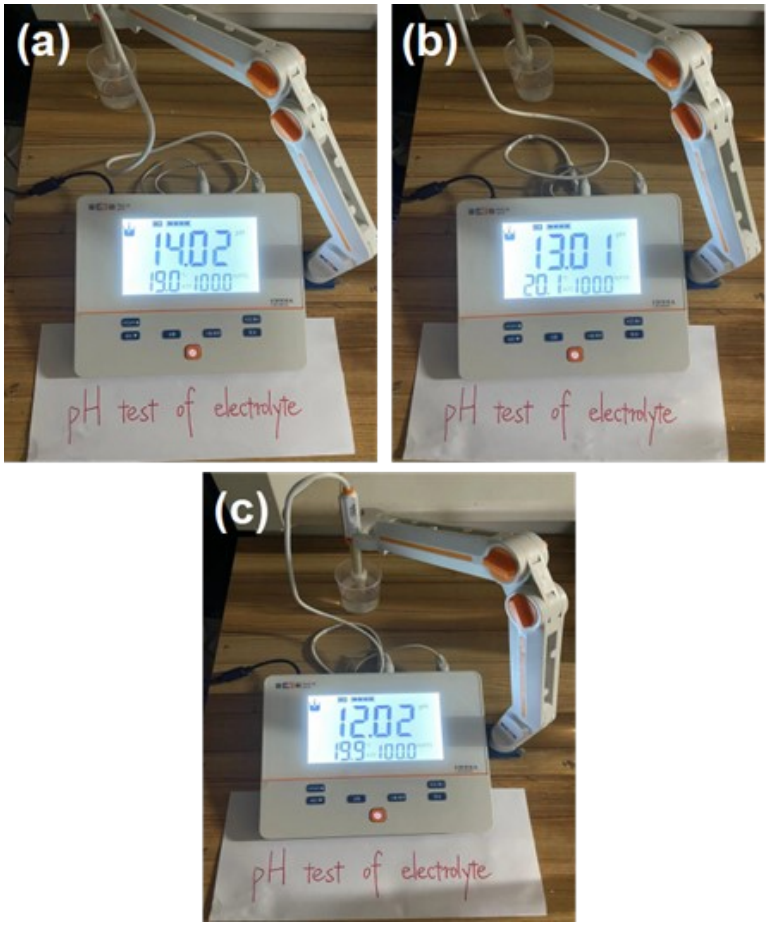


**Figure S17.** The pH test photo of electrolytes with (a) 1 M KOH, (b) 0.1 M KOH and (c) 0.01 M KOH.

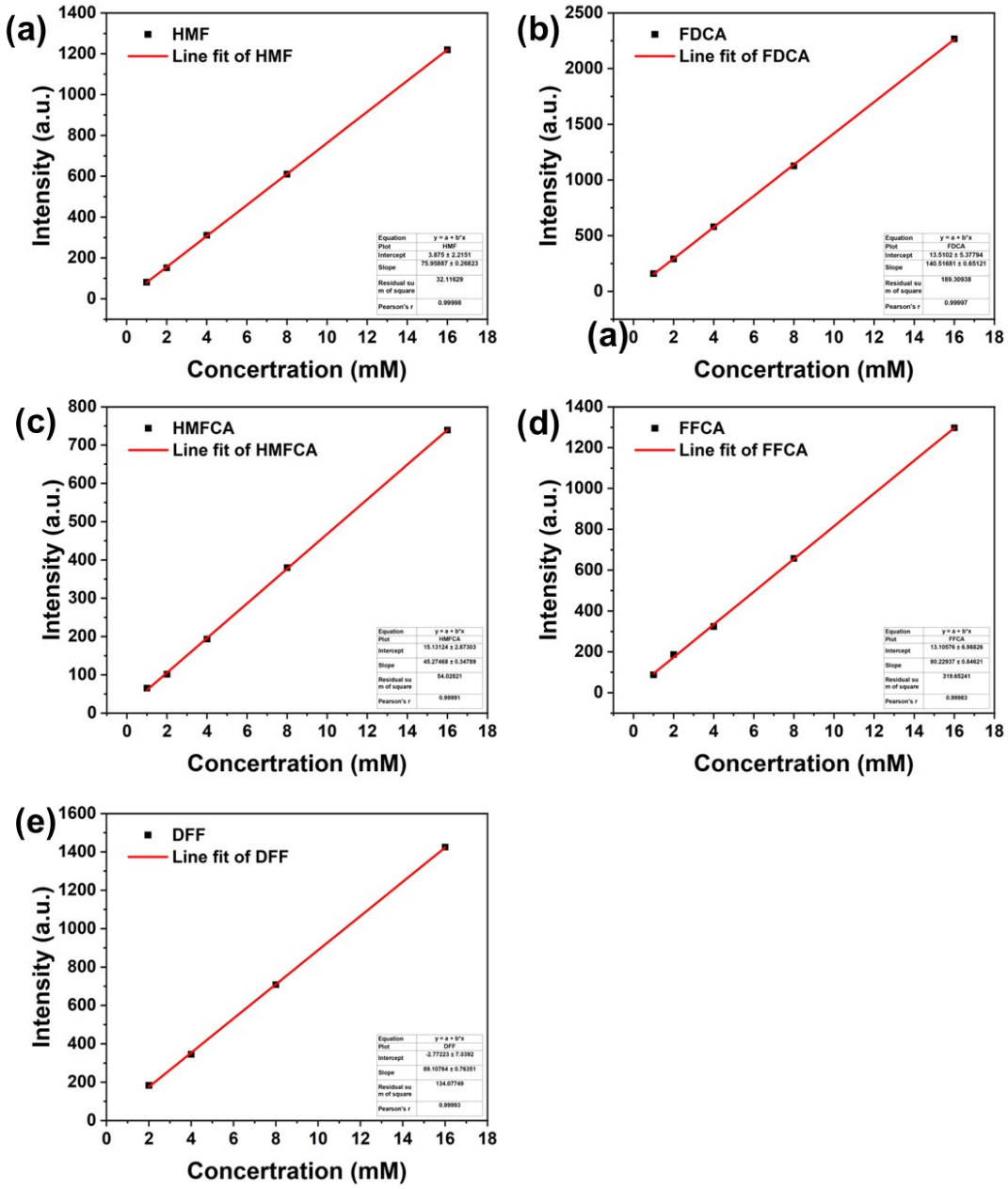


**Figure S18.** Standard peak-concentration fitting curve. (a) HMF, (b) FDCA, (c) HMFCA, (d) FFCA, (e) DFF.

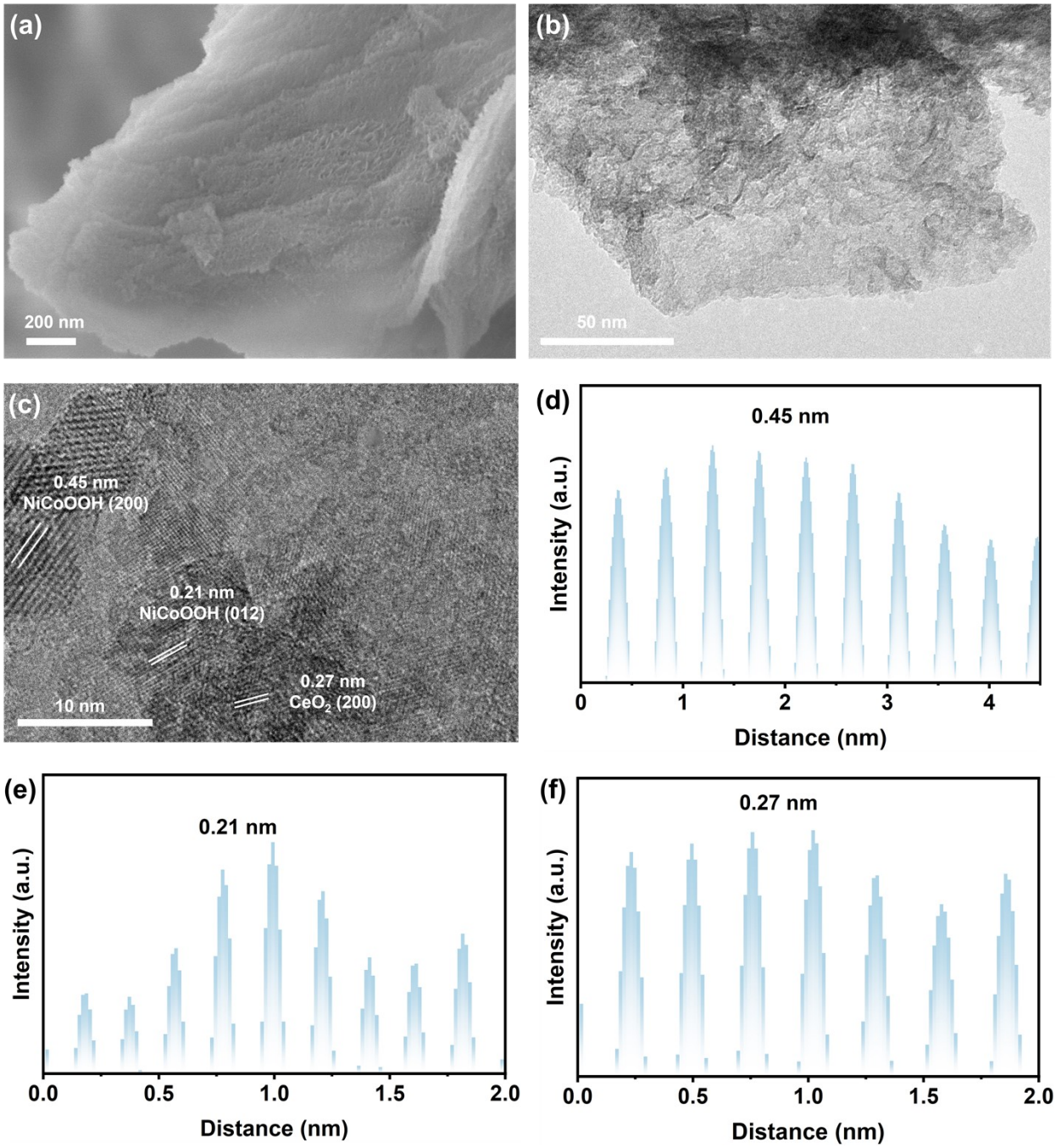


**Figure S19.** (a) SEM, (b) TEM, (c) HRTEM images, (d) NiCoOOH (200) crystal plane, (e) NiCoOOH (012) crystal plane and (f) $CeO_2$ (200) crystal plane interplanar spacing of $CeO_2$/NiCoOOH after 5 cycles of electrolysis.

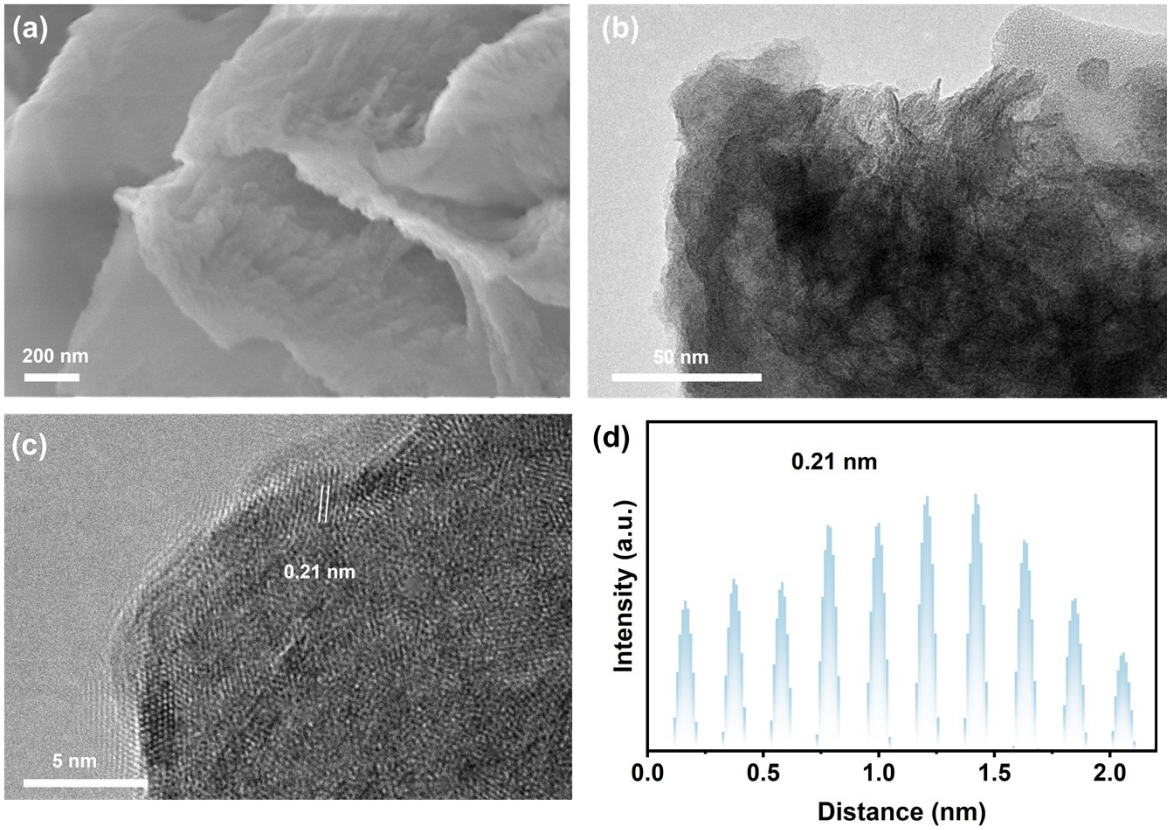


**Figure S20.** (a) SEM, (b) TEM, (c) HRTEM images and (d) the corresponding interplanar spacing of the NiCoOOH sample after 5 cycles of electrolysis.

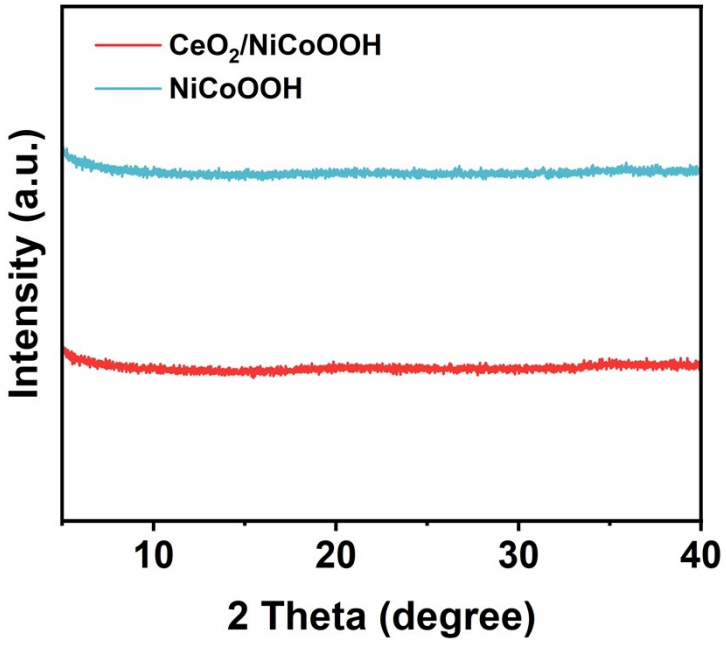


**Figure S21.** XRD pattern of the $CeO_2$/NiCoOOH and NiCoOOH sample after 5 cycles of electrolysis.

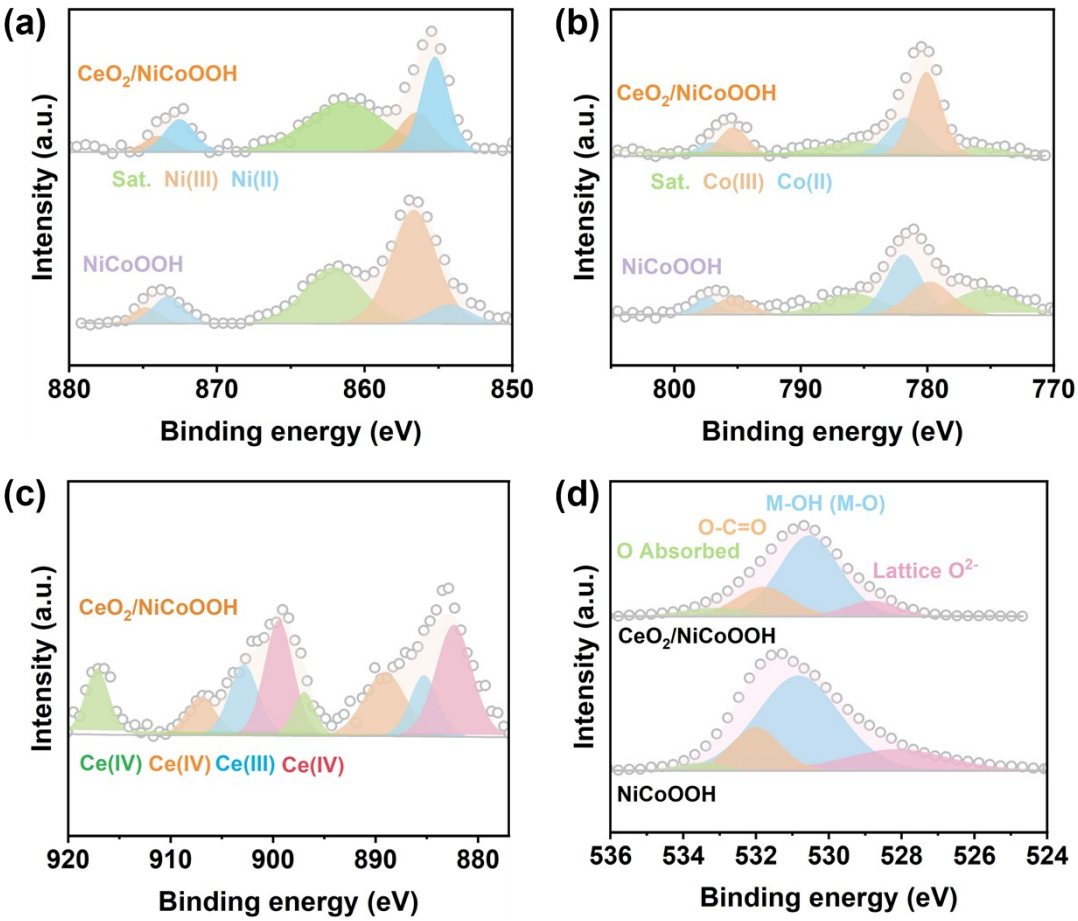


**Figure S22.** XPS spectra of the (a) Ni 2p, (b) Co 2p, (c) Ce 3d, and (d) O 1s for NiCoOOH and $CeO_2$/NiCoOOH after 5 cycles of electrolysis.

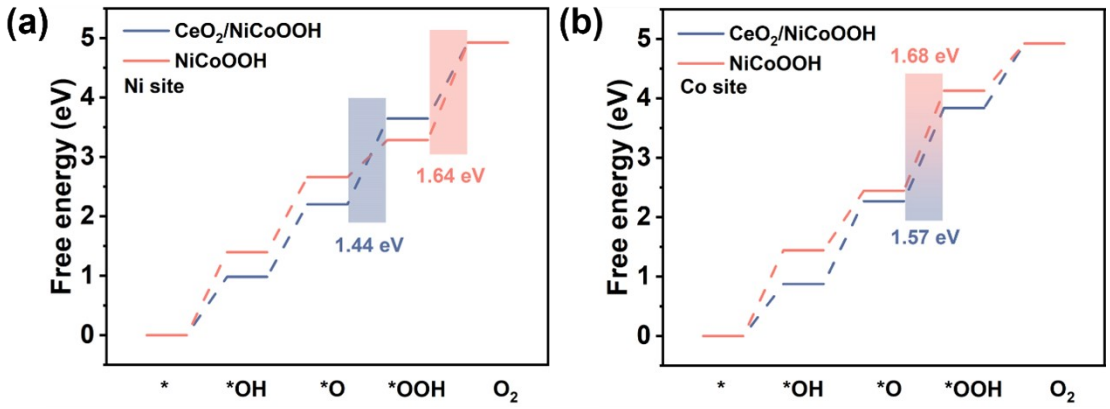


**Figure S23.** Free energies of (a) Ni and (b) Co sites on NiCoOOH and $CeO_2$/NiCoOOH by OER.

**Table S1** ICP-OES results of NiCo-MOF and NiCoCe-MOF before and after activation

| Samples | Atomic Ratio (Ni/Co/Ce) |
|---|---|
| NiCo-MOF | 1:0.57:0 |
| NiCoOOH(NF) | 1:0.08:0 |
| NiCoCe-MOF | 1:0.69:0.53 |
| $CeO_2$/NiCoOOH(NF) | 1:0.07:0.02 |

**Table S2.** The amount of Ni, Co, Ce element in the solution after the reaction

| Sample | Ni(mmol) | Co(mmol) | Ce(mmol) |
|---|---|---|---|
| $CeO_2$/NiCoOOH(NF) | 0.029 | 0.027 | 0.007 |

**Table S3.** Comparison of activity for $CeO_2$/NiCoOOH and other reported catalysts.

| Electrode Materials | Potential | HMF conversion (%) | FDCA yield (%) | Faradaic efficiency (%) | Ref. |
|---|---|---|---|---|---|
| NiCoBDC-NF | 1.55 $V_{RHE}$ | / | 99 | 78.8 | J. Mater. Chem. A, 2020, 8, 20386–20392. |
| NiCoFeS-MOF | 1.39 $V_{RHE}$ | 100 | 99 | 99 | J. Mater. Chem. A, 2023, 11, 6375–6383. |
| CoNiFe-MOFs/NF | 1.4 $V_{RHE}$ | / | 99.76 | 100 | J. Mater. Chem. A, 2021, 9, 14270–14275. |
| NiCo-MOF | 1.35 $V_{RHE}$ | 100 | 97.3 | 90 | Chem. Eng. J., 2024, 484, 149768. |
| NiO | 1.5 $V_{RHE}$ | / | 92.42 | 90.35 | ACS Catal. 2022, 12, 4242–4251. |
| $NiS_X$/β-$Ni(OH)_2$/Ni | 1.413 $V_{RHE}$ | 97.7 | / | 98.3 | Adv, Mater. 2023, 35, 2211177. |
| av-$Ni(OH)_2$/CP | 1.45 $V_{RHE}$ | 98.97 | 98.51 | 98.46 | Chem. Eng. J., 2023, 477, 146917. |
| CoNiTe | 1.50 $V_{RHE}$ | 97 .0 | / | 91.1 | J. Colloid Interface Sci. 2024, 670, 96–102 |
| $Co_3O_4$-NiO | 1.45 $V_{RHE}$ | 96.95 | 83.33 | 89.47 | Chem. Eng. J., 2024, 481, 148303. |
| FeCoNi-LDH | 1.45 $V_{RHE}$ | 95.68 | 94.83 | 94.71 | Chem. Eng. J., 2024, 481, 148429. |
| NiOOH | 1.55 $V_{RHE}$ | 95.92 | 89.71 | / | Adv. Sci. 2023, 10, 2302641. |
| NiCoLDH/NF | 1.32 $V_{RHE}$ | 100 | / | 96 | Energy Environ. Sci., 2023, 16, 5305–5314. |
| Ce-NiFe | 1.42 $V_{RHE}$ | 88.5 | 83.1 | 91.0 | Adv. Energy Mater. 2024, 2400676 |
| NiCoFe-LDHs | / | 95.5 | 84.9 | ~90.0 | ACS Catal. 2020, 10, 5179−5189. |
| **$CeO_2$/NiCoOOH** | **1.4 $V_{RHE}$** | **95.87** | **95.22** | **99.26** | **This work** |